Association between the Analytical Technique and Finite Element Method for designing SPMSMs with Inner Rotor Type for Electric Vehicle Applications

Duc-Quang Nguyen
Faculty of Electrical Engineering, Electric Power University, Vietnam
quangndhtd@epu.edu.vn

Thanh Nguyen Thai
Hitachi Energy VietNam Company Limited, Vietnam
Thanh.NT231182M@sis.hust.edu.vn

Cuc Le Thi
Hitachi Energy VietNam Company Limited, Vietnam
Cuc.LT231173M@sis.hust.edu.vn

Dinh Bui Minh
School of Electrical and Electronic Engineering, Hanoi University of Science and Technology, Vietnam
dinh.buiminh@hust.edu.vn

Vuong Dang Quoc
School of Electrical and Electronic Engineering, Hanoi University of Science and Technology, Vietnam
vuong.dangquoc@hust.edu.vn (corresponding author)

Received: 16 February 2024 | Revised: 5 March 2024 | Accepted: 6 March 2026

 DOI: https://doi.org/10.48084/etasr.7087

ABSTRACT

This paper focuses on computing the electromagnetic parameters of inner rotor-configuration Surface-mounted Permanent Magnet Synchronous Motors (SPMSMs) via the combination of analytical and finite element methods with an application to electric bicycles. The analytical method is, first, developed in detail to calculate the essential parameters of the inner rotor-configuration SPMSM. Then, a Finite Element Method (FEM) is introduced to verify the analytical parameters found. Further, a simulation of magnetic flux density, torque, cogging torque, torque ripple, back Electromagnetic Force (EMF), linkage flux, and temperature is performed. The end result is validated with a real 2.2 kW inner rotor-configuration SPMSM.

Keywords-permagnent magnet synchronous motor; inner rotor type; analytical method; finite element method

I. INTRODUCTION

Throughout the decades, the world has grappled with various environmental challenges, including global warming and air pollution. A significant contributor to air pollution is the burning of fossil fuels in cars. Apart from the environmental concerns, issues such as traffic congestion and escalating oil prices have prompted many nations to explore alternative, eco-friendly modes of transportation, such as Electric Vehicles (EVs). Among the array of EVs, the electric bicycle stands out as a suitable option for short-distance travel due to its appealing attributes such as affordability, ease of riding, convenient parking, health benefits and environmental friendliness [1-4]. The electric motor used in electric bicycles plays a pivotal role, necessitating careful design to ensure high efficiency, torque, and reduced noise. A developing area of research is the investigation of motor types such as the Permanent Magnet Synchronous Motor (PMSM), Multi-Flux Permanent Magnet (MFPM), Switched Reluctance Motor (SRM) and Permanent Magnet Flux Switched Motor (PMFSM)

in terms of their efficiency [5-8]. These motors are characterized by a compact size and a light weight due to the absence of brushes in their design. The rotor design commonly falls into two categories: a) those with an inner rotor, fitting between the two cranks and chain wheel, and b) those with an outer rotor, fitting into the wheel.

Our research will focus on the Surface-mounted PMSM (SPMSM) with inner-rotor configuration as shown in Figure 1. Our primary aim is to develop an analytical method – supplemented by a Finite Element Method (FEM) – to design the SPMSM with an inner rotor. Our calculation will estimate the magnetic flux density, torque, cogging torque, torque ripple, back electromagnetic force (EMF), linkage flux and temperature of the motor. Those results, will, then, be validated on a real 2.2 kW inner rotor-configuration SPMSM.

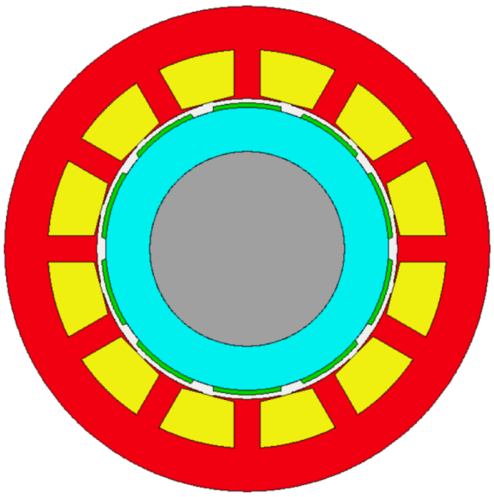

Fig. 1. SPMSM with an inner rotor configuration.

II. BACKGROUND AND ANALYTICAL DESIGN

For the calculation, we have assumed the following input parameters for the SPMSM with inner rotor structure (Table I):

TABLE I. INPUT PARAMETERS OF SPMSM WITH INNER ROTOR CONFIGURATION.

Description	Value
Imput power (P_{rated})	2200 W
Rated voltate (U_{rated})	380 V
Efficiency (η)	90%
Frequency (f_{rated})	50 Hz
Power factor ($cos\varphi$)	0.9
Number of pole pairs (p)	5
Phase number (m)	3
Speed of rotor (n)	600 rpm
Number slot per pole per phase (q)	0.4

A. Design of the Stator

Based on the parameters given in Table I, the rated torque (T_{rated}) is calculated via the rated power (P_{rated}) and the number of pole pairs (p), as follows [9]:

$$T_{rated} = \frac{p.P_{rated}}{2\pi.f_{rated}} \quad (1)$$

The inner diameter of the stator is defined via the rated torque as [9]:

$$D_{ins} = \sqrt[3]{V_0.T_{rated}} \quad (2)$$

where V_0 is a factor depending on the method of cooling of the machine. This factor can be defined as [9, 13]:

$$V_0 = 5 - 7\ \frac{in^3}{ft.lb} = 61375 - 85925\ \frac{mm^3}{Nm} \quad (3a)$$

if the rated power is less than 10 Hp and:

$$V_0 = 2 - 5\ \frac{in^3}{ft.lb} = 24550 - 61375\ \frac{mm^3}{Nm} \quad (3b)$$

if the rated power is more than 10 Hp.

The stator length is given by:

$$L_{act} = \frac{V_0.T_{rated}}{D_{in}^{\ 2}} \quad (4)$$

The height of the stator yoke is defined as:

$$h_{sy} = \frac{\phi_{sy}}{B_{sy}.L_{act}.k_j} \quad (5)$$

where k_j is the superposition factor ($k_j = 0{,}96$), B_{sy} and ϕ_{sy} correspond to the flux density and magnetic flux of stator yoke respectively. It should be noted that the $\phi_{sy} = \frac{\phi_m}{2}$.

Accordingly, the height of rotor yoke is given by:

$$h_{ry} = \frac{\phi_{ry}}{B_{ry}.L_{act}.k_j} \quad (6)$$

where B_{ry} and ϕ_{ry} are the flux density and magnetic flux of the rotor yoke. It should be noted that the $\phi_{ry} = \frac{\phi_m}{2}$.

B. Design of the Inner Rotor

The stator slots are defined as a function of the input parameters as:

$$Q_s = 2.m.p.q \quad (7)$$

where m is the phase number and q is the slot number per pole per phase.

The cover angle of the Permanent Magnet (PM) (α_m) is defined via the cover thickness of the PM (e_m) ($e_m = 0{,}7$) as:

$$\alpha_m = e_m.\pi \quad (8)$$

The flux density of the PM is defined [9-12] as:

$$B_m = \propto_m . B_{r,m} \quad (9)$$

where $\propto_m$ is the PM factor ($\propto_m = 0{,}6 \div 0{,}95$) and $B_{r,m}$ is the PM remanent.

The thickness of the PM (h_m) is then computed as [9]:

$$h_m = \frac{\mu_r.\delta}{\frac{B_{r,m}.4.sin\alpha_m}{B_g.\pi} - 1} \quad (10)$$

where μ_r is the relative permeability of the PM and δ is the air length. The remanent of PM ($B_{r,m}$) is determined by the following expression [10, 11]:

$$B_{r,m} = B_{r,0}\left(1 - T_k(T_r - T_0)\right) \quad (11)$$

where $B_{r,0}$ is the remanent of the PM at the ambient temperature, T_k is the temperature factor, T_r is the PM temperature at the stage operation and T_0 is the ambient temperature. The air flux density (B_g) is then defined as:

$$B_g = \frac{4}{\pi}.B_m.sin\alpha_m \quad (12)$$

The inner diameter of the rotor is:

$$D_{inr} = D_{ins} - 2(h_m + \delta) \quad (13)$$

The width of the PM is calculated as a function of e_m and D_{inr}, as:

$$W_m = \frac{e_m.D_{inr}.\pi}{p} \quad (14)$$

The magnetic flux of the PM is, then, defined as:

$$\phi_m = B_m.W_m.L_{act} \quad (15)$$

The magnetic field on the tooth of the stator is defined as:

$$\phi_{tooth} = \frac{p.\phi_m}{Q_s} \quad (16)$$

where Q_s corresponds to the stator slots and ϕ_m is the PM magnetic flux.

The width of the stator tooth is:

$$w_{tooth} = \frac{\phi_{tooth}}{B_{tooth}.L_{act}.k_j} \quad (17)$$

where B_{tooth} and ϕ_{tooth} are the magnetic flux density and magnetic flux on the tooth, respectively.

Finally, the pole pitch (τ_s) is defined as:

$$\tau_s = \frac{\pi.D_{in}}{Q_s} \quad (18)$$

C. *Design of the Windings*

The winding factor (k_{dq}) is chosen from Figure 2. The area of the winding (S_d) is calculated as [9, 20]:

$$S_d = \frac{I_p}{J.a} \quad \text{and} \quad d = \sqrt{\frac{4.S_d}{\pi.b}} \quad (19)$$

where I_p is the phase current, J is the electric current density and a is the number of parallel branches.

The number of turns is, then, calculated as:

$$n_s = \frac{1{,}1.U_p}{2\sqrt{2}.\pi.f_s.q.k_{dq}.B_g.cos\gamma.D.L_{act}} \quad (20)$$

where γ is the torque angle.

The upper diameter of the slot is:

$$b_{s0} = \frac{\pi.(D_{is}+2.h_{os}+2.h_w)}{Q_s} - w_{tooth} \quad (21)$$

The lower diameter of the slot is:

$$b_{s2} = \sqrt{4.A_{slot}.\tan\frac{\pi}{Q_s} + b_{so}^2} \quad (22)$$

The height of the slot is:

$$h_s = \frac{2.A_{slot}}{b_{s0}+b_{s2}} \quad (23)$$

Finally, the outer diamter of stator becomes:

$$D_{outs} = D_{inr} + 2.(h_{sy} + h_w + h_{s0}) \quad (24)$$

Q_s		Poles 4	6	8	10	12	14	16	20	22	24	26
6	ξ_1	**0.866**	**	0.866	0.5	**	0.5	0.866	0.866	0.5	**	0.5
	q	0.5		0.25	0.2		0.143	0.125	0.1	0.091		0.077
9	ξ_1		**0.866**	**0.945***	**0.945***	**0.866**	0.617	0.328	0.328	0.617	0.866	0.945
	q		0.5	0.375	0.3	0.25	0.214	0.188	0.15	0.136	0.125	0.115
12	ξ_1			0.866	0.933	**	0.933	0.866	0.5	0.25	**	0.25
	q			0.5	0.4		0.286	0.25	0.2	0.182		0.154
15	ξ_1				0.866	**	**0.951***	**0.951***	0.866	0.711	**	0.39
	q				0.5		0.357	0.313	0.25	0.227		0.192
18	ξ_1					**0.866**	0.902	0.945	0.945	0.902	0.866	0.74
	q					0.5	0.429	0.375	0.3	0.273	0.25	0.231
21	ξ_1						0.866	0.89	**0.953***	**0.953***	**	0.89
	q						0.5	0.438	0.35	0.318		0.269
24	ξ_1							0.866	0.933	0.949	**	**0.949**
	q							0.5	0.4	0.364		0.308

$q > 0.5$

Fig. 2. Winding factors.

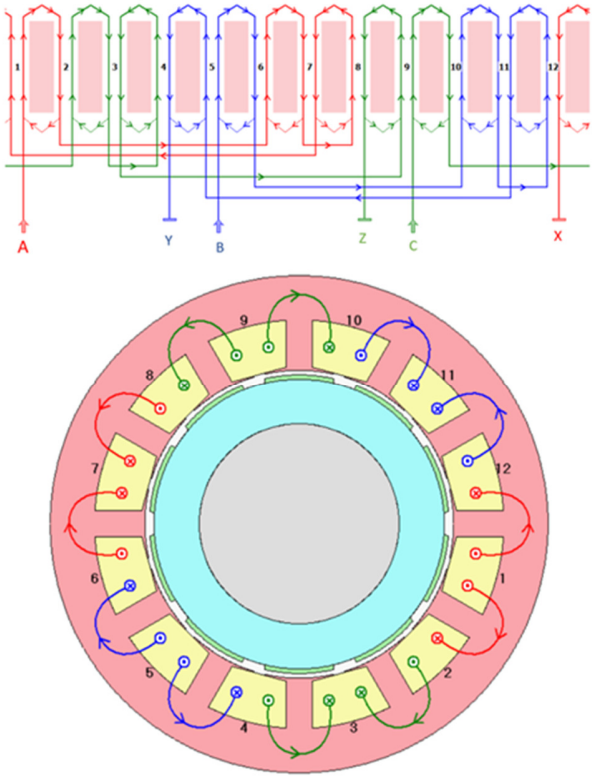

Fig. 3. Diagram of the stator windings (top) and the cross-section of the motor (bottom).

III. FINITE ELEMENT APPROACH

The analytical model, outlined above, provides a quick calculation of design parameter variations. However, this model only allows for the estimation of the main parameters and main sizes. Thus, a FEM implementation becomes necessary. The Maxwell equations in Euclidean space $\mathbb{R}^3$ are [9]:

$$\nabla \times \mathbf{H} = \mathbf{J}_s \quad (25a)$$

$$\nabla \times \mathbf{E} = -j\omega\,\mathbf{B} \quad (25b)$$

$$\nabla \cdot \mathbf{B} = 0 \quad (25c)$$

where $\mathbf{J}_s$ is the current density (A/m^2), $\mathbf{H}$ is the magnetic field (A/m), $\mathbf{E}$ is the electric field (V/m) and $\mathbf{B}$ is the magnetic flux density (T).

The above equations (25a-b-c) are solved with constitutive laws and boundary conditions (BCs) as [9]:

$$\mathbf{B} = \mu \mathbf{H} \quad (26a)$$

$$\mathbf{J} = \sigma \mathbf{E} \quad (26b)$$

$$\boldsymbol{n} \times \mathbf{H}|_{\Gamma_h} = 0 \quad (27a)$$

$$\boldsymbol{n} \cdot \mathbf{B}|_{\Gamma_e} = 0 \quad (27b)$$

where $\mathbf{J}$ is the eddy current density (A/m^2), μ and σ are the relative permeability and electric conductivity (S/m) respectively and $\boldsymbol{n}$ is the unit normal exterior to Ω (with $\Omega = \Omega_c \cup \Omega_c^c$ corresponding to the domain of a PM machine). It should be noted that the field $\mathbf{B}$ in (25c) is derived from a vector potential $\mathbf{A}$ as:

$$\boldsymbol{B} = \nabla \times \boldsymbol{A} \quad (28)$$

By combining (25b) and (28), the field $\mathbf{E}$ is defined via an electric scalar potential φ as follows:

$$\mathbf{E} = -\partial_t \mathbf{A} - \nabla \cdot \varphi \quad (29)$$

The weak form equation is derived from equations (25) to (28) [9, 14-17] as:

$$\nabla \times \left[\frac{1}{\mu}(\nabla \times \mathbf{A} - \mathbf{B})\right] + \sigma \partial_t \mathbf{A} = \mathbf{J}_s - \sigma \nabla \cdot \varphi \quad (30)$$

The linkage flux (ϕ) is, then, defined as:

$$\phi = \frac{L}{S}\left(\iint_{\Omega+} \mathbf{A} d\Omega - \iint_{\Omega-} \mathbf{A} d\Omega\right) \quad (31)$$

where L is the length and S is the cross section area of the conductor. The back EMF can be, readily, defined as:

$$e = \frac{L}{S}\left(\iint_{\Omega+} \partial_t \mathbf{A} d\Omega - \iint_{\Omega-} \partial_t \mathbf{A} d\Omega\right) \quad (32)$$

IV. NUMERICAL TEST

Based on the input parameters given in Table I, the analytical method is, first, employed to define the essential parameters of the 2.2 kW inner rotor configuration SPMSM. The analytical results are given in Table II.

TABLE II. ANALYTICAL RESULTS

Description	Value	Unit
Outer diameter of stator	217.8	mm
Inner diameter of stator	135	mm
Outer diameter of rotor	128	mm
Inner diameter of rotor	92.2	mm
Length of stator	135	mm
Number of stator slots	12	Rãnh
Air gap	1	mm
Thickness of PM	2.5	mm
Efficiency	94.505	%
Torque	35.315	Nm
Power factor	0.967	
Output power	2218.9	W
Total losses (on load)	129.02	W

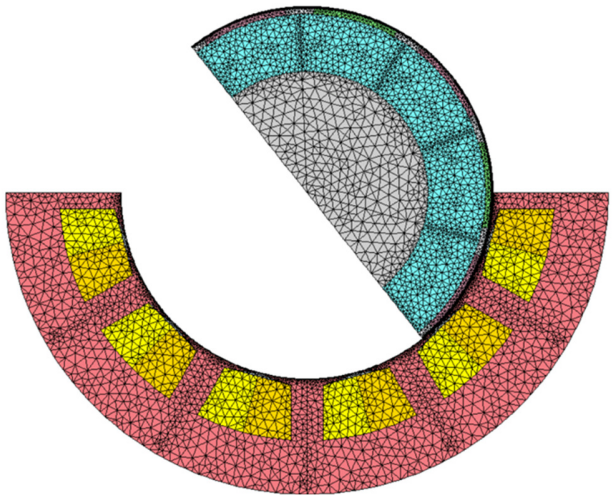

Fig. 4. Model of 2D mesh for both stator and rotor.

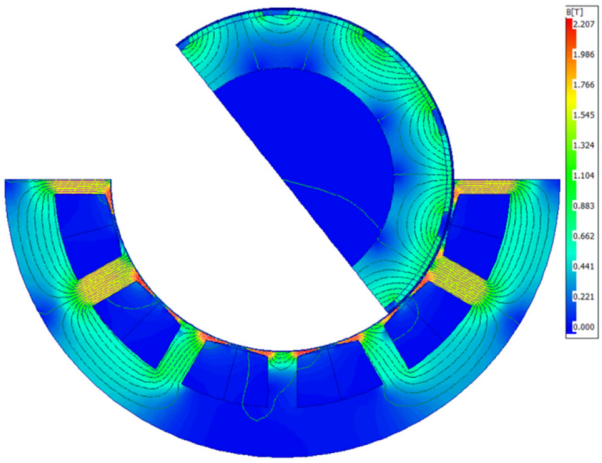

Fig. 5. Distribution of magnetic flux density in both stator and rotor.

Then, the FEM is introduced to verify and simulate the electromagnetic parameters of this motor. The model of the 2-D mesh for both rotor and stator is shown in Figure 4. The distribution of the magnetic flux density in both the stator and rotor can be seen in Figure 5. It becomes evident that the maximum value of $\mathbf{B}$ goes up to 2.207 T. The distribution of the linkage flux is shown in Figure 6. It can be assumed that its waveform is rather smooth and sinusoidal.

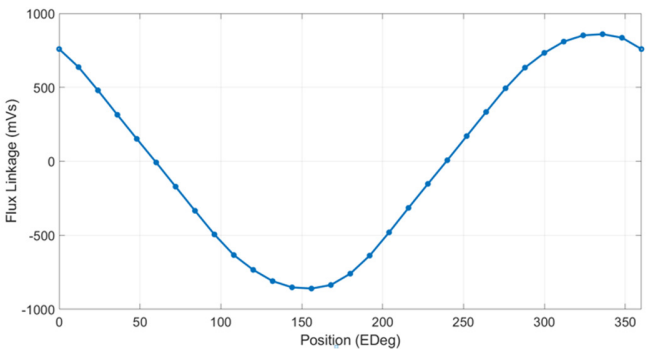

Fig. 6. The linkage flux waveform.

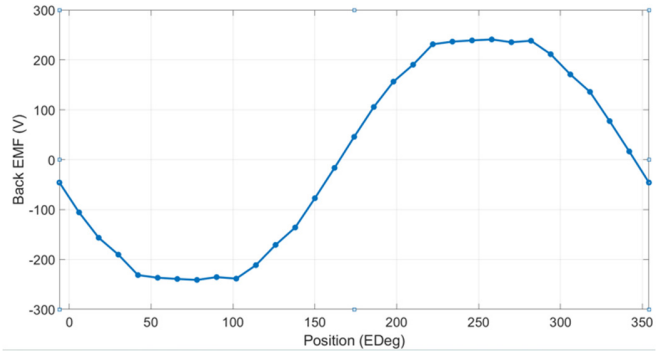

Fig. 7. The back EMF waveform.

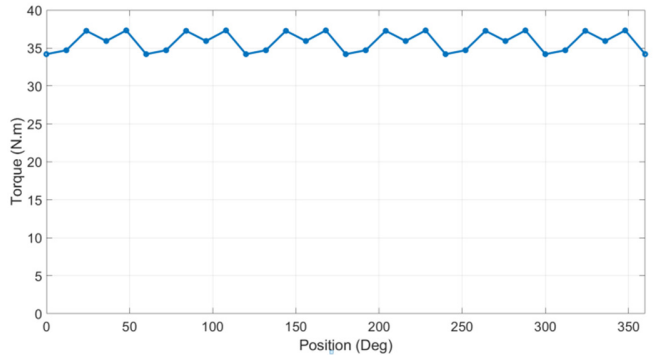

Fig. 8. The output torque waveform.

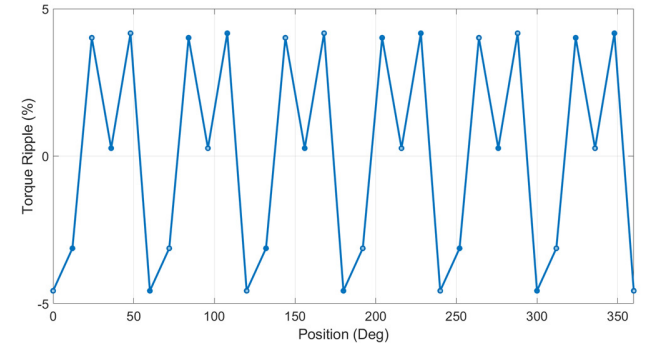

Fig. 9. The torque ripple waveform.

The distribution waveform of back EMF is shown in Figure 7. It can be observed that its waveform is almost sinusoidal with small harmonic components. Figure 8 depicts the waveform of the output torque. The maximum value is 37.5 N.m with an average value of 36 N.m. The torque ripple is shown in Figure 9. The value is smaller than 5.1 %. The torque ripple plays a crucial role in the design. One major factor contributing to torque ripple is the cogging torque, as depicted in Figure 10.

The results indicate that the machine reached a fair level of stability guaranteeing its smooth operation. As for the noise and vibration of the motor, these can be attributed, mainly, to the cogging torque. Figure 11 shows the temperature distribution map of the equivalent thermal circuit inside the machine. The radial and axial views of the thermal model are illustrated in Figures 12 and 13, respectively. It can be seen that the motor's maximum temperature is 75.4 ^{0}C.

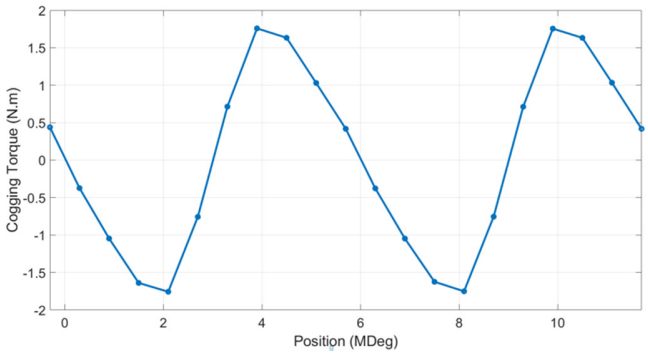

Fig. 10. The flux cogging torque waveform.

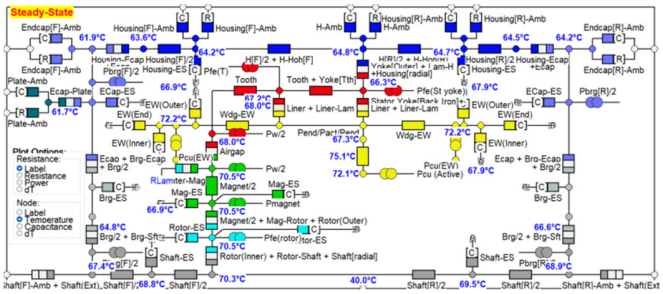

Fig. 11. Thermal equivalent magnetic circuit.

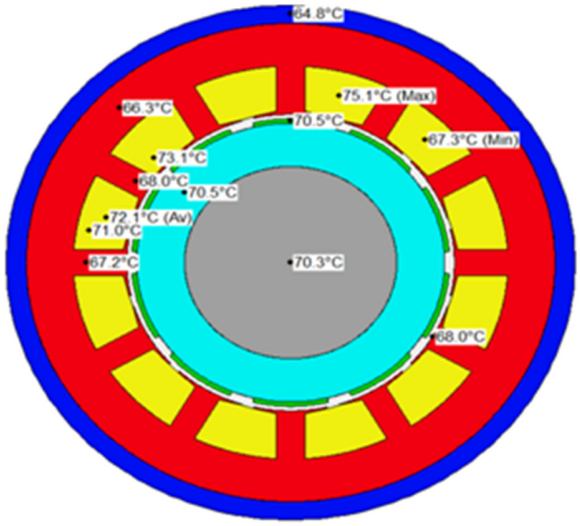

Fig. 12. Radial view of the thermal model.

V. CONCLUSION

We have successfully designed a 2.2 kW SPMSM of the inner rotor type, combining an analytical model with FEM. The required specifications of the motor were computed via the analytic approach, followed by the FEM in order to verify and simulate parameters such as the magnetic flux density, linkage flux, back EMF, output torque, torque ripple and cogging torque. The results obtained can be considered as reference data for designers, researchers, and manufacturers providing the

suitable prototype design of an SPMSM with an inner rotor type. Furthermore, the employment of FEM, allowed for the thermal model to be developed, via the equivalent magnetic circuit, so as for the temperature distribution inside the motor to be estimated. This work lays the groundwork for future studies, potentially involving optimization methods like genetic or swarm algorithms in order to refine the design calculations.

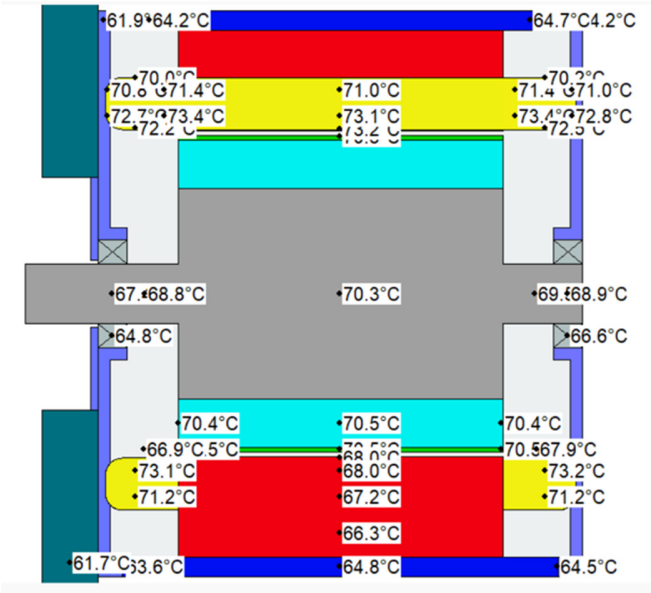

Fig. 13. Axial view result of the thermal model.

ACKNOWLEDGMENT

This research is funded by Hanoi University of Science and Technology (HUST) under project number T2023-PC-043.

REFERENCES

[1] H. M. Taha and I. Alnaab, "Designs of PMSMs with Inner and Outer Rotors for Electric Bicycle Applications," *Kurdistan Journal of Applied Research*, vol. 4, no. 1, pp. 20–25, Jun. 2019, https://doi.org/10.24017/science.2019.1.4.

[2] S. B. Bhat, S. P. Nikam, and B. G. Fernandes, "Design and analysis of ferrite based permanent magnet motor for electric assist bicycle," in *2014 International Conference on Electrical Machines (ICEM)*, Sep. 2014, pp. 106–111, https://doi.org/10.1109/ICELMACH.2014.6960166.

[3] P. Zhang, G. Y. Sizov, and N. A. O. Demerdash, "Comparison of torque ripple minimization control techniques in Surface-Mounted Permanent Magnet Synchronous Machines," in *2011 IEEE International Electric Machines & Drives Conference (IEMDC)*, May 2011, pp. 188–193, https://doi.org/10.1109/IEMDC.2011.5994641.

[4] J.-Y. Choi, H.-I. Park, J. Seok Myeong, and S.-H. Lee, "Design and Analysis of Surface-Mounted PM Motor of Compressor for Electric Vehicles Applications according to Slot/Pole Combinations," *The Transactions of The Korean Institute of Electrical Engineers*, vol. 60, pp. 1846–1857, Oct. 2011, https://doi.org/10.5370/KIEE.2011.60.10.1846.

[5] T. H. Manh, D. B. Minh, T. P. Minh, and V. D. Quoc, "Investigation of the Influence of Skewed Slots and Degmagnetization Effects to Line Start Permanent Magnet Assistance Synchronous Reluctance Motors," *Engineering, Technology & Applied Science Research*, vol. 13, no. 1, pp. 9807–9811, Feb. 2023, https://doi.org/10.48084/etasr.5307.

[6] L. Feng, S. Yu, F. Zhang, S. Jin, and Y. Sun, "Study on performance of low-speed high-torque permanent magnet synchronous motor with dynamic eccentricity rotor," *Energy Reports*, vol. 8, pp. 1421–1428, Aug. 2022, https://doi.org/10.1016/j.egyr.2022.03.018.

[7] J. Lin, N. Schofield, and A. Emadi, "External-rotor 6–10 switched reluctance motor for an electric bicycle," in *IECON 2013 - 39th Annual Conference of the IEEE Industrial Electronics Society*, Nov. 2013, pp. 2839–2844, https://doi.org/10.1109/IECON.2013.6699581.

[8] T. F. Chan, L.-T. Yan, and S.-Y. Fang, "In-wheel permanent-magnet brushless DC motor drive for an electric bicycle," *IEEE Transactions on Energy Conversion*, vol. 17, no. 2, pp. 229–233, Jun. 2002, https://doi.org/10.1109/TEC.2002.1009473.

[9] H. Vu Xuan, "Modeling of Exterior Rotor Permanent Magnet Machines with Concentrated Windings," Ph.D. dissertation, Electrical Engineering, Mathematics and Computer Science, Technische Universiteit Delft, Delft, Netherlands, 2012.

[10] S. J. Kim, E.-J. Park, S.-Y. Jung, and Y.-J. Kim, "Transfer Torque Performance Comparison in Coaxial Magnetic Gears With Different Flux-Modulator Shapes," *IEEE Transactions on Magnetics*, vol. 53, no. 6, pp. 1–4, Jun. 2017, https://doi.org/10.1109/TMAG.2017.2663429.

[11] W.-S. Jung, H.-K. Lee, Y.-K. Lee, S.-M. Kim, J.-I. Lee, and J.-Y. Choi, "Analysis and Comparison of Permanent Magnet Synchronous Motors According to Rotor Type under the Same Design Specifications," *Energies*, vol. 16, no. 3, Jan. 2023, Art. no. 1306, https://doi.org/10.3390/en16031306.

[12] Z. Q. Zhu and D. Howe, "Influence of design parameters on cogging torque in permanent magnet machines," *IEEE Transactions on Energy Conversion*, vol. 15, no. 4, pp. 407–412, Dec. 2000, https://doi.org/10.1109/60.900501.

[13] X. Liu, Z. Zhang, J. Xiao, and H. Xu, "Comparison and analysis of electromagnetic characteristics of IPMSM with single and double layer PMs," *International Journal of Applied Electromagnetics and Mechanics*, vol. 58, no. 4, pp. 483–496, Jan. 2018, https://doi.org/10.3233/JAE-180032.

[14] J. Dong, Y. Huang, L. Jin, and H. Lin, "Comparative Study of Surface-Mounted and Interior Permanent-Magnet Motors for High-Speed Applications," *IEEE Transactions on Applied Superconductivity*, vol. 26, no. 4, pp. 1–4, Jun. 2016, https://doi.org/10.1109/TASC.2016.2514342.

[15] T. Pu, G. Du, J. Tong, N. Huang, N. Li, and W. Xu, "Comparison of Rotor Strength of Various Rotor Structures for Ultra-high-speed Permanent Magnet Synchronous Motor," in *2021 IEEE 4th Student Conference on Electric Machines and Systems (SCEMS)*, Dec. 2021, pp. 1–6, https://doi.org/10.1109/SCEMS52239.2021.9646110.

[16] M. Sahebjam, M. B. Bannae Sharifian, M. R. Feyzi, and M. Sabahi, "Novel Unified Control Method of Induction and Permanent Magnet Synchronous Motors," *International Journal of Engineering*, vol. 32, no. 2, pp. 256–269, 2019.

[17] V. K. B. Ponnam and K. Swarnasri, "Multi-Objective Optimal Allocation of Electric Vehicle Charging Stations and Distributed Generators in Radial Distribution Systems using Metaheuristic Optimization Algorithms," *Engineering, Technology & Applied Science Research*, vol. 10, no. 3, pp. 5837–5844, Jun. 2020, https://doi.org/10.48084/etasr.3517.